Biomaterials Science

ROYAL SOCIETY OF CHEMISTRY

PAPER

View Article Online
View Journal | View Issue



Cite this: *Biomater. Sci.*, 2023, **11**, 7432

# Fluid flow-induced modulation of viability and osteodifferentiation of periodontal ligament stem cell spheroids-on-chip†

Apurva Mishra, [a] Ren Kai, [b,c] Srividya Atkuru, [a] Yichen Dai, [a] Filippo Piccinini, [d,e] Philip M. Preshaw [f] and Gopu Sriram *[a,g]

Developing physiologically relevant *in vitro* models for studying periodontitis is crucial for understanding its pathogenesis and developing effective therapeutic strategies. In this study, we aimed to integrate the spheroid culture of periodontal ligament stem cells (PDLSCs) within a spheroid-on-chip microfluidic perfusion platform and to investigate the influence of interstitial fluid flow on morphogenesis, cellular viability, and osteogenic differentiation of PDLSC spheroids. PDLSC spheroids were seeded onto the spheroid-on-chip microfluidic device and cultured under static and flow conditions. Computational analysis demonstrated the translation of fluid flow rates of 1.2 μl $min^{-1}$ (low-flow) and 7.2 μl $min^{-1}$ (high-flow) to maximum fluid shear stress of 59 μPa and 360 μPa for low and high-flow conditions, respectively. The spheroid-on-chip microfluidic perfusion platform allowed for modulation of flow conditions leading to larger PDLSC spheroids with improved cellular viability under flow compared to static conditions. Modulation of fluid flow enhanced the osteodifferentiation potential of PDLSC spheroids, demonstrated by significantly enhanced alizarin red staining and alkaline phosphatase expression. Additionally, flow conditions, especially high-flow conditions, exhibited extensive calcium staining across both peripheral and central regions of the spheroids, in contrast to the predominantly peripheral staining observed under static conditions. These findings highlight the importance of fluid flow in shaping the morphological and functional properties of PDLSC spheroids. This work paves the way for future investigations exploring the interactions between PDLSC spheroids, microbial pathogens, and biomaterials within a controlled fluidic environment, offering insights for the development of innovative periodontal therapies, tissue engineering strategies, and regenerative approaches.

Received 15th June 2023,
Accepted 4th October 2023

DOI: 10.1039/d3bm01011b

rsc.li/biomaterials-science



## Introduction

Periodontitis, characterized by persistent chronic inflammation in response to the dysbiotic subgingival biofilm, results in the destruction of the periodontal ligament (PDL) and surrounding alveolar bone. With a worldwide prevalence exceeding 50%, advanced forms of this disease rank as the sixth most prevalent condition globally,[1] contributing to tooth loss, impaired mastication, diminished quality of life, and potential systemic complications.[2,3] Moreover, it imposes a substantial economic burden, with estimated annual costs of USD 154 billion in the United States and €159 billion in Europe.[4]

PDL is a specialized dense fibrous connective tissue that anchors the tooth roots to the alveolar bone of the jaws. Beyond its anchorage role, PDL plays a crucial role in tooth eruption, physiological mobility during mastication, proprioception, and bone remodeling.[5] These dynamic and highly ordered tissues are regulated by mechanosensitive mechanisms, with mechanical forces such as those from mastication playing a crucial in maintaining PDL and alveolar bone homeostasis.[5,6] Cells within the PDL, including periodontal ligament stem cells (PDLSCs), respond to mechanical stimuli, influencing tissue remodeling, regeneration, and repair.[7,8] Mechanical loading on teeth results in the compression of the

[a]*Faculty of Dentistry, National University of Singapore, Singapore. E-mail: sriram@nus.edu.sg*
[b]*State Key Laboratory of Fluid Power and Mechatronic Systems, School of Mechanical Engineering, Zhejiang University, Hangzhou, Zhejiang, PR China*
[c]*Key Laboratory of Advanced Manufacturing Technology of Zhejiang Province, School of Mechanical Engineering, Zhejiang University, Hangzhou, Zhejiang, PR China*
[d]*IRCCS Istituto Romagnolo per lo Studio dei Tumori (IRST) "Dino Amadori", Meldola, Italy*
[e]*Department of Medical and Surgical Sciences (DIMEC), University of Bologna, Bologna, Italy*
[f]*School of Dentistry, University of Dundee, Dundee, UK*
[g]*NUS Centre for Additive Manufacturing (AM.NUS), National University of Singapore, Singapore*

† Electronic supplementary information (ESI) available. See DOI: https://doi.org/10.1039/d3bm01011b

interstitial fluid within the PDL space, generating fluid shear stress on both cells and extracellular matrix (ECM).[9,10] Similarly, mechanical stress on the alveolar bone leads to interstitial fluid flow within the lacuna-canalicular network, affecting bone remodeling responses of osteocytes within the network.[11,12] Both mechanical stimuli and dynamic interstitial fluid flow actively contribute to the maintenance and turnover of PDL and alveolar bone.[13–15] Additionally, interstitial fluid flow plays a crucial role in maintaining tissue homeostasis by facilitating nutrient and oxygen delivery, waste removal, and the transport of signaling molecules.[16] While the flow of interstitial fluid is driven by hydrostatic and osmotic pressure differences between blood, interstitial tissues, and lymphatics, mechanical loading of the tooth provides an active driving force. Unlike the osteocytes within the lacuna-canalicular network, cells within soft tissues usually experience extremely low fluid shear stress, ranging from $10^{-3}$ to $10^{-1}$ dyne per $cm^2$ (*i.e.*, 10 to 1000 μPa), due to the relatively slow interstitial fluid flow.[17,18]

Although traditional static monolayer cultures have provided valuable insights into the biological responses of PDL fibroblasts, PDLSCs, and osteoblasts to microbial challenge and biomaterials, there is growing recognition of the importance of replicating native microenvironmental characteristics in *in vitro* testing. Specifically, the inclusion of fluid flow, cell–cell, and cell–matrix interactions within the experimental setup is widely acknowledged to provide enhanced physiological relevance.[19,20] Hence, applying fluid flow within *in vitro* cultures, which in turn provides fluid shear stress-induced mechanotransduction would enable partial emulation of native physiology of the PDL compared to static cultures. Studies on the incorporation of active fluid flow over monolayer-cultured PDL cells have demonstrated the impact of fluid shear stress on the rearrangement of cytoskeletal proteins,[21,22] modulation of tissue remodeling,[21] and immunoregulatory properties,[23] and production of growth factors, messenger molecules, and chemokines.[16,21,24] Interstitial fluid flow also enhances the osteogenic differentiation potential of monolayer-cultured PDL cells,[21,22,25,26] pre-osteoblasts,[27,28] and mesenchymal stromal cells (MSCs).[29–31] Although these studies demonstrate the impact of mechanical stress and fluid flow using monolayer cultures, the three-dimensional (3D) microenvironment of the cell–cell and cell–matrix interactions are not represented.

3D cultures provide unique opportunities to emulate physiologically relevant cell–cell and cell–matrix interactions, establish native tissue-like nutrient and oxygen gradients, and elicit heterogenous cellular responses, surpassing the limitations of monolayer cultures.[32,33] Numerous studies have demonstrated wide differences between monolayer and 3D cultures, wherein 3D spheroids of the dental pulp and PDL cells exhibit enhanced osteogenic differentiation and periodontal regeneration compared to their monolayer counterparts.[34–37] However, the static microenvironment of conventional microwell or hanging drop culture plates results in rapid depletion of nutrients and oxygen, and the formation of a hypoxic core.[38,39] Furthermore, the impact of mechanical stress and fluid flow are not represented in static spheroid 3D cultures. Bioreactors provide a platform for continuous movement of culture medium either on top of cells attached to microcarriers,[40,41] or through a microporous biomaterial loaded with cells.[42,43] Although perfusion bioreactors emulate physiological features such as dynamic nutrient supply and fluid shear stress, they demand the need for a large number of cells and culture medium, and experienced operators. These limitations could be overcome using microfluidic systems.

Microfluidics technology utilizes microchannels and microchambers, enabling the manipulation of fluid composition, precise control of micro-sized fluid volumes and shear stress.[44] Using a microfluidic approach, cells can be cultured confined within micro-sized channels and chambers. This microscale confinement offers a physiologically relevant microenvironment compared to traditional macroscale cultures. The convergence of microfluidic technology and 3D culture models provides new possibilities to culture cellular aggregates or tissue equivalents within a confined microchamber, precisely control the fluid flow, shear stress, chemical and physical gradients, enabling the potential to emulate the native 3D microenvironment of the tissue.[38,44–46] Only recently, the application of microfluidics for dental, oral, and craniofacial research has gained traction.[47] For instance, the flow feature has been used to mimic the interstitial fluid flow through gingival connective tissue,[45] apply mechanical stress on gingival tissues,[48,76] simulate the protective effects of gingival crevicular fluid flow,[45] and emulate host–microbe interactions.[45,49] Similarly, it has been utilized to mimic the nutrient provision and metabolic waste or toxic product removal role of the blood vessels.[50,51,76]

The aim of this study was to integrate the culture of PDLSC spheroids within a spheroid-on-chip microfluidic perfusion platform and to investigate the impact of interstitial fluid flow on morphogenesis, cellular viability, and osteogenic differentiation of PDLSC spheroids.

# Methods

### Cell culture

PDLSCs were isolated from the root surfaces of de-identified, healthy, non-carious, impacted third molars extracted from systemically healthy donors (15–30 years old) with informed consent. The study was approved by the National Healthcare Group Doman Specific Review Board Singapore (Study Reference Number: 2018/00256). The cells were isolated from tissue fragments scraped from the middle one-third of the roots. The tissue fragments were cultured under animal component-free (ACF) conditions as explants in culture vessels coated with MesenCult™-ACF cell attachment substrate (StemCell Technologies) in Mesencult™-ACF complete medium (StemCell Technologies), supplemented with 1% glutamax (Gibco), 1% penicillin–streptomycin (Gibco) and 0.50 μg $mL^{-1}$ amphotericin-B (Gibco). The PDLSCs isolated under ACF conditions were expanded under the same media conditions

without amphotericin-B, and characterized for the expression of surface markers using flow cytometry as described previously.[52]

### Spheroid generation and culture within the microfluidic device

For the generation of spheroids, PDLSCs of passages 4–5 from a single donor were used. PDLSCs were dissociated using ACF dissociation reagents (MesenCult™ ACF Dissociation Kit; StemCell Technologies), seeded at a density of 10 000 cells per well in 96-well round bottom ultra-low attachment plates (Corning), force aggregated using low-speed centrifugation (20*g*, 1 min) and incubation at 37 °C for 24 hours.

Following 24 hours of organization, the spheroids were transferred to sterile µ-Slide spheroid microfluidic perfusion chips (ibidi GmbH). Each chip (25 mm × 75 mm; individually sterile packed) contained 3 parallel, identical perfusion channels, each with an array of 7 identical microwells (volume: 3.5 µl per well) (Fig. 1). An exploded cross-sectional view of a single microwell with dimensions of the perfusion channel, microwell and coverslip covering the bottom and top is shown in Fig. 1A. The width and height of the flow-in microchannels connecting the 7 microwells were 1 mm and 0.2 mm, respectively. The distance between the centres of 2 adjacent microwells were 4.5 mm. Each microwell, had a niche area for the spheroid culture, the dimensions of which were 800 µm in diameter and 400 µm in height. Each fluidic channel had dedicated inlet and outlet ports that connect to inlet and outlet tubing for perfusion of culture media. Before connecting to the chip, the tubing and connectors were disinfected with 70% ethanol followed by perfusion of autoclaved distilled water and sterile basal culture media to remove remnants of alcohol from the tubing. The spheroids were individually placed onto the bottom of each microwell. The channels and microwells were sealed using a sterile, polymer-based adhesive film (ibidi GmbH) as per manufacturer's instructions. For culture under flow conditions to generate continuous fluidic shear stress on the spheroids within the microwells, the chip was connected to inlet and outlet tubings, and media was actively perfused using a digitally-controlled peristaltic pump (Ismatec, Cole-Parmer), at a defined pulse rate of 0.88 pulses per minute. The peristaltic pump fitted with tubings of internal diameters of 0.25 mm and 0.76 mm was used to deliver pulsatile low-flow (1.2 µl $min^{-1}$) and high-flow (7.2 µl $min^{-1}$) conditions respectively. For culture under static conditions, the inlet and outlet ports were fitted with a 1 ml syringe as media reservoirs, filled with equal media volumes, and the media was manually changed every alternate day.

### Numerical simulation and fluid shear stress modeling

Computational fluid dynamics of fluidic flow inside the microfluidic chips (velocity profiles, flow streamline, and fluid shear

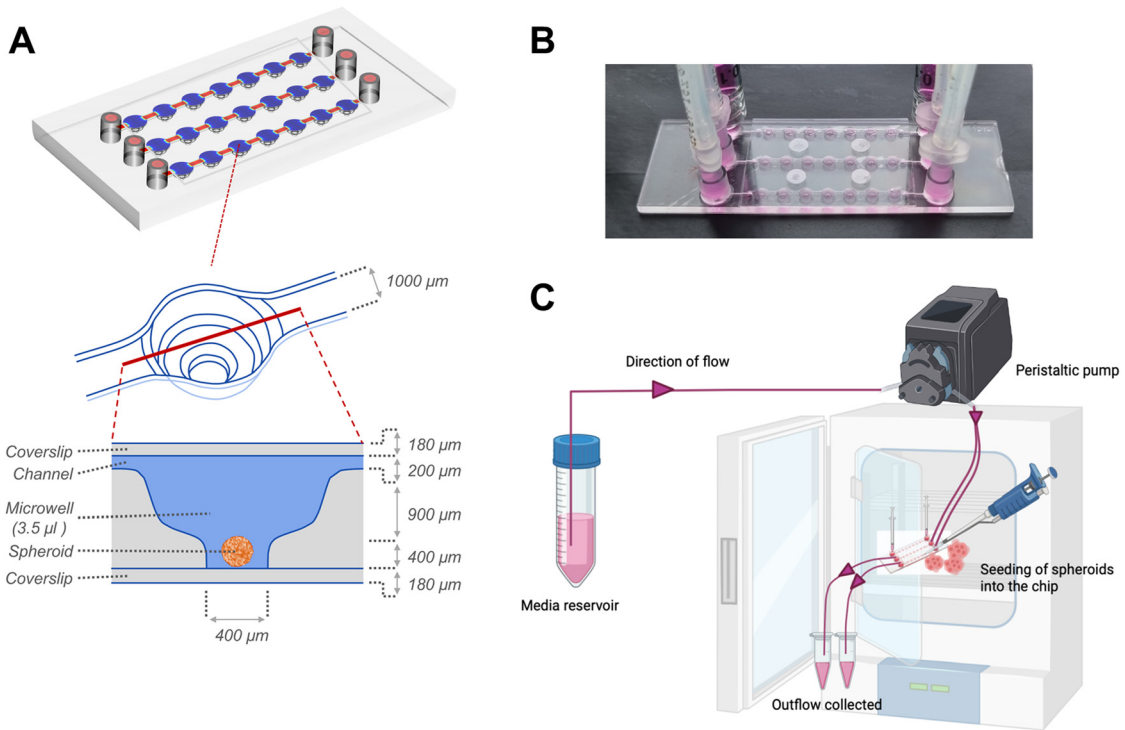


**Fig. 1** Spheroid-on-chip microperfusion platform. (A) Schematic representation of the microfluidic perfusion device illustrating three parallel channels, each with seven microwells and ports at both ends of each channel to facilitate the media flow. The enlarged cross-sectional views show the dimensions of the microwell (*adapted from ibidi GmbH*). (B) Photograph of the microfluidic device after seeding the spheroids and securing the connections to enable the flow of media. (C) Schematic representation of the microfluidic perfusion set-up and application of the unidirectional flow through the microfluidic device using a peristaltic pump.

stress profiles) was performed using COMSOL Multiphysics® simulation tool. 3D geometric models of the microfluidic device based on the dimensions of the channels and microwells provided in Fig. 1A were used for laminar flow simulations. Briefly, the Navier–Strokes equation was used to determine the fluid velocity and shear stress.[53]

$$\rho(u\nabla)u = \nabla \cdot [-\rho I + \mu(\nabla u + (\nabla u))T] + F + \rho g$$

where $u$ is the velocity vector of the fluid, $\rho$ the fluid density, $\mu$ the dynamic viscosity, $F$ the external force acting on the fluid ($F = 0$ in the model), $T$ the temperature, and $g$ the acceleration due to gravity. Cell culture media was assumed to be identical to pure water with a density of 1000 kg $m^{-3}$ and viscosity of 0.001 kg $m^{-1}$ $s^{-1}$. Inlet velocity was set as the inflow velocity calculated according to the flow conservation defined by the pump.

### Morphometric assessment of spheroids

The spheroids cultured under static and flow conditions were imaged at different time points using a brightfield microscope (Olympus IX83). Morphometric parameters (maximum diameter and surface area of the spheroids) were computed using measurement tool functions in CellSens imaging software (Olympus). The 2D brightfield images of the spheroids were used to create volumetric 3D reconstruction of the spheroids using ReViSP (Reconstruction and Visualization using a Single Projection), an open-source software.[54]

### Live/dead staining and apoptosis assessment

The spheroids within the microfluidic device were rinsed with phosphate-buffered saline (PBS), stained on-chip for 20 minutes with a solution containing Hoechst (NucBlue Live ready probes, Thermo-Fisher Scientific), calcein-AM (1 μg $ml^{-1}$, Thermo-Fisher Scientific) and propidium iodide (PI, 1 μg $ml^{-1}$, Thermo-Fisher Scientific) for labelling the nuclei, live and dead cells, respectively. Whole-mount imaging of the spheroids on-chip was captured using laser scanning confocal microscopy (FV1000, Olympus). *Z*-Stacks of the images were reconstructed using Imaris software (Oxford instruments). The numbers of dead cells at defined *z*-planes were quantified using ImageJ software (NIH, USA). Further, cellular apoptosis was quantified fluorometrically using caspase-3/7 activity (SensoLyte Homogeneous AFC Caspase – 3/7 assay kit, AnaSpec) as per manufacturer's recommendations. Briefly, the spheroids were incubated with 50 μl of assay working solution at 37 °C for 1 hour. Caspase 3/7-mediated conversion of the assay substrate was measured fluorometrically using a microplate reader ($\lambda_{ex}$: 354 nm, $\lambda_{em}$: 442 nm).

### Evaluation of osteodifferentiation potential

Spheroids cultured on-chip were exposed to osteodifferentiation (OD) media (MesenCult™ osteogenic differentiation kit, StemCell Technologies) under continuous unidirectional perfusion. Osteodifferentiation potential was assessed after 10 and 14 days of differentiation. At each time point, the spheroids were harvested from the chip and lysed using passive lysis buffer (Promega) based on manufacturer's instructions, and sonicated for 10 seconds. Intracellular alkaline phosphatase (ALP) activity was measured using SensoLyte pNPP alkaline phosphatase assay colorimetric kit (AnaSpec), which is a biochemical assay based on the conversion of *p*-nitrophenyl phosphate into *p*-nitrophenol in the presence of ALP. ALP activity was calculated by measuring the optical absorbance at 405 nm using a microplate reader and correlating to a standard curve of known concentrations of *p*-nitrophenol. The same cell lysate was used to quantify intracellular osteocalcin (OCN) and DNA quantity using a human osteocalcin ELISA kit (R&D Systems) and a Quant-iT PicoGreen dsDNA assay kit (Invitrogen), respectively, as per the manufacturer's protocol. ALP activity and OCN levels were normalized using DNA quantity from the same cell lysate.

To further evaluate the mineralization potential, the spheroids cultured for 14 days in osteogenic conditions were fixed with 4% neutral-buffered formalin (Sigma) for 20 min, followed by PBS rinse twice. The fixed spheroids were stained with 40 mM alizarin red (Sigma-Aldrich) for 20 min and washed three times with PBS to remove the unbound stain. The stained spheroids were imaged using a brightfield microscope. The staining intensity (red colour) was quantified using ImageJ software.[55]

Spheroids cultured on-chip for 14 days in osteogenic conditions were incubated overnight with calcium binding agent IRDye® 800CW BoneTag™ (2 pmol $ml^{-1}$, Li-COR Biosciences, USA) at 4 °C.[56] After incubation, spheroids were washed twice with PBS, counterstained with DAPI and visualized using a laser scanning microscope (Stellaris, Leica Microsystems).

### Statistical analysis

Statistical analysis was performed using GraphPad Prism (version 9.3, USA). The Shapiro–Wilk test was used to assess normality (alpha = 0.05), followed by one-way analysis of variance (ANOVA) and *post-hoc* Tukey tests to determine significant differences between groups. The data were represented as mean ± SD, and differences were considered statically significant when $p < 0.05$. The experiments were performed in replicates represented by "*n*" in respective figure legends.

## Results

### Spheroid-on-chip design and numerical simulation

The microfluidic device used in this study comprised three parallel, independent channels, each with seven microwells for the spheroid culture, connected with individual inlet and outlet ports (Fig. 1). The channels had the same height of 100 μm, and all the microwells had an identical bowl-like shape with a cylindrical microchamber at the bottom to house the spheroids. Each independent channel provided the opportunity to model different fluid shear stress parameters by varying the input flow rates using the digitally-controlled peristaltic pump.

To mimic interstitial fluid shear stress, two different perfusion flow rates of 1.2 μl $min^{-1}$ (low flow) and 7.2 μl $min^{-1}$ (high flow) were used to generate different shear stresses in the culture channels. These flow rates equated to an inlet velocity of 0.1 mm $s^{-1}$ and 0.6 mm $s^{-1}$ for the low and high-flow conditions, respectively. Based on Stokes law, velocities and shear rates are linearly proportional to flow rates. Hence, colorimetric maps of velocity and shear stress profiles of the high flow only are presented in Fig. 2A and B. Assuming zero outlet pressure, the maximum velocity within the channels connecting the microwells was computed as 161.63 μm $s^{-1}$ and 969.57 μm $s^{-1}$ for low and high-flow conditions, respectively. Numerical calculations presented in the velocity profiles demonstrate the gradient in the fluid flow streamlines from the top to the bottom of each well. As the spheroids are expected to settle downwards and be housed within the cylindrical microchamber at the bottom of each microwell (niche area), we calculated the fluid shear stress at different *z*-planes of the microwell. Fig. 2B plots the fluid shear stress at *z*-planes of 200, 500, and 1000 μm from the top of the microwell, which shows the generation fluid shear stress of different magnitudes within the microwells on-chip (Fig. 2C). The maximum fluid shear stress experienced at the bottom of the microwells ($z$ = −1000 μm), was computed as 59 μPa and 360 μPa for low and high-flow conditions, respectively (Fig. 2D). These extremely low fluid shear stress levels correlate with the physiological limits of interstitial fluid flow in soft tissues (10 to 1000 μPa).[17,18]

### Effect of fluid flow on the morphology of PDLSC spheroids

PDLSCs isolated under ACF conditions were characterized for the expression of mesenchymal (CD73, CD90, CD105), major histocompatibility complex (HLA-ABC and HLA-DR) and hematopoietic (CD31, CD34, CD45) markers. The PDLSCs showed >98% of the cells positive for the expression of classical surface proteins CD73, CD90 and CD105, >87% of the cells positive for HLA-ABC with no significant expression of HLA-DR, CD31, CD34, CD45 and STRO-1 (ESI Fig. S1†).

Brightfield microscopic images of spheroids cultured under static and flow conditions within the microfluidic chips were used to understand the changes in spheroid morphology over time (Fig. 3A and B). The round spheroid morphology was gen-

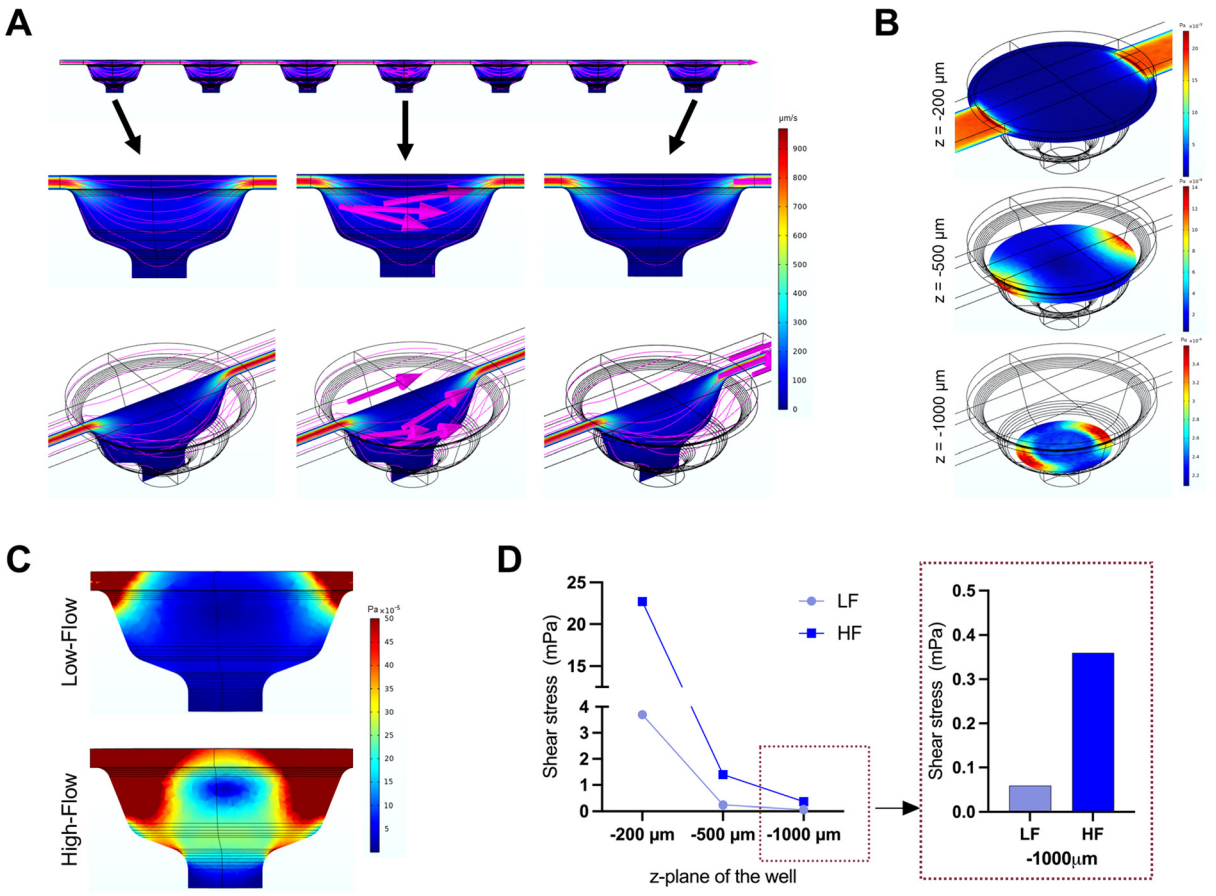


**Fig. 2** COMSOL simulations of flow on the microfluidic chip. (A) Colorimetric map of velocity profiles at a uniform inlet velocity (0.6 mm $s^{-1}$) and outlet pressure (0 Pa) representative of high-flow conditions (HF). (B) Colorimetric map of fluid shear stress profile at different *z*-planes of the microwell for HF conditions. (C) Fluid shear stress profile along a cross-sectional plane perpendicular to fluid flow for low-flow (LF) and HF conditions. (D) Graph depicting the variation in maximum fluid shear stress across different *z*-planes inside the microwell under different flow conditions (S: static, LF: low-flow, HF: high-flow).

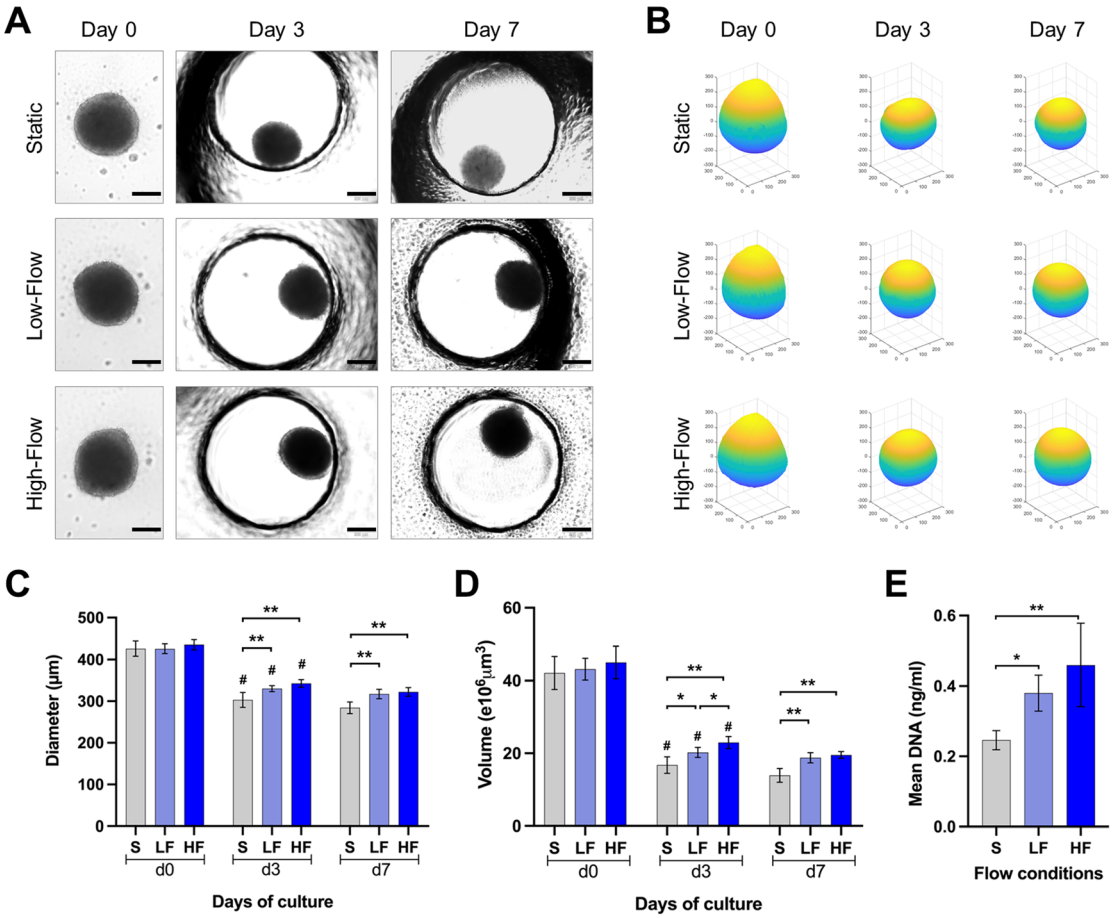


**Fig. 3** Morphological characterization of PDLSC spheroids cultured on-chip under different flow conditions. (A) Representative brightfield images of the PDLSC spheroids cultured from day 0–7 under different flow conditions (scale bar: 200 μm) and (B) their volumetric reconstruction. Graphs illustrating the flow-induced change in the (C) diameter and (D) reconstructed volume of the spheroids over culture duration. (mean ± SD, *$p < 0.05$, ** $p < 0.01$, $n \geq 6$), (d0 *vs.* d3 of respective culture condition, $^{\#}p < 0.01$). (E) Graph showing DNA quantification from the spheroids at day 7 under different flow conditions (mean ± SD, *$p < 0.05$, $n = 5$) (S: static, LF: low-flow, HF: high-flow).

erally maintained under static and flow conditions. Analysis of spheroid diameter and reconstructed volume revealed dynamic changes over the culture period in all three flow conditions (Fig. 3C and D). Initially, at day 0, spheroids exhibited a relatively uniform diameter and volume across all the three conditions. On day 3, a substantial decrease in spheroid diameter and volume was observed in all the three conditions. Notably, the diameter of the spheroids cultured under high and low-flow conditions was significantly larger than those under static conditions on day 3. On day 7, the changes in spheroid dimensions were minimal. After 7 days of culture, the spheroids cultured under high-flow conditions showed the highest diameter and reconstructed volume, followed by those under low-flow and static conditions (Fig. 3C and D). However, there were no significant difference in the spheroid dimensions between low and high-flow conditions. These findings were further corroborated by higher DNA content among the spheroids cultured under low and high-flow conditions (on day 7), reflecting the finding of larger spheroids observed under flow conditions (Fig. 3E).

### Impact of fluid flow on cellular viability of PDLSC spheroids

Confocal microscopic imaging of the spheroids stained with calcein-AM and PI demonstrated the presence of viable and dead cells, respectively. *Z*-Projections of the confocal images of the spheroids after 7 days of culture showed a reduced number of dead cells under flow conditions compared to no flow (Fig. 4A and B). To understand the effect of flow on the necrotic core, we quantified the number of dead cells at different *z*-planes from the periphery towards the spheroid core at depths of 10, 35, and 55 μm from the periphery. Spheroids cultured for 24 h under flow conditions showed lower amounts of dead cells compared to those cultured under static conditions. This effect was more pronounced in deeper *z*-planes (Fig. 4C). Though the total number of dead cells increased among all the conditions on day 7, the trend was more pronounced with significantly lower amounts of dead cells in the spheroid core under flow conditions compared to static conditions (Fig. 4C). These findings were corroborated with significantly lower amounts of caspase 3/7 activity in the spheroids (on day 7) cul-

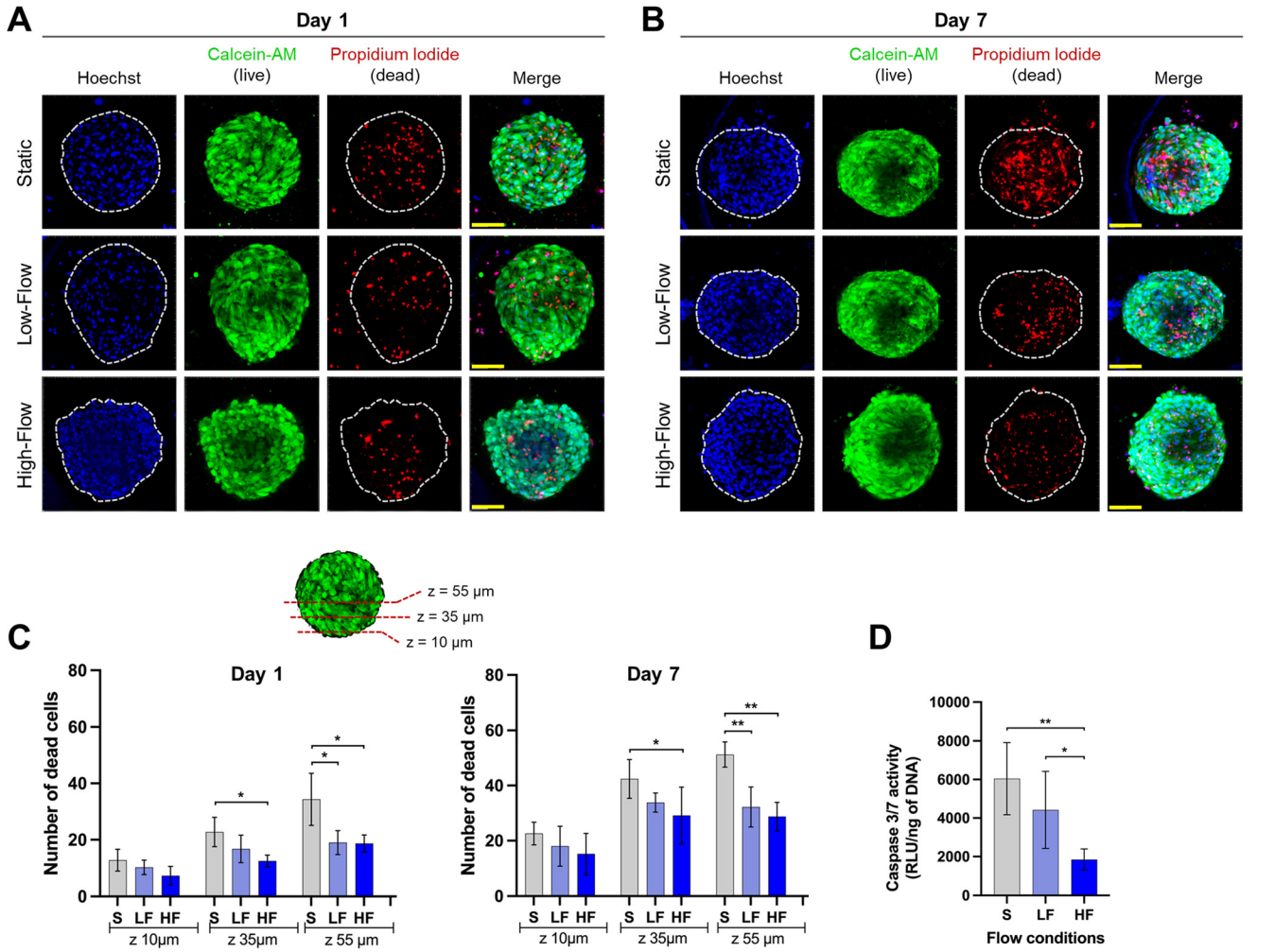


**Fig. 4** Cellular viability of PDLSC spheroids under flow conditions. Representative confocal *z*-projection of PDLSC spheroids (blue: nuclei stained with Hoechst, green: live cells stained with calcein AM and red: dead cells stained with propidium iodide) at: (A) day 1 (24 hours after flow initiation) and (B) day 7 of the culture (scale bar: 100 µm). (C) Quantification of number of dead cells at different *z*-planes (from periphery to core of spheroid) after 1 and 7 days of initiation of flow (mean ± SD, $*p < 0.05$, $** p < 0.01$, $n \geq 4$). (D) Quantification of caspase 3/7 activity (normalized with DNA) at day 7 of the culture on-chip (mean ± SD, $*p < 0.05$, $** p < 0.01$, $n \geq 5$). (S: static, LF: low-flow, HF: high-flow).

tured under flow conditions compared to static conditions (Fig. 4D). Though, there were no significant differences in the number of dead cells between low and high-flow conditions, caspase 3/7 activity levels were significantly lower in high-flow conditions compared to low-flow conditions. Overall, these findings suggest the improved viability of spheroids cultured under flow conditions potentially due to flow-induced active perfusion of culture media into the spheroids.

### Effect of fluid flow modulation on osteodifferentiation potential of PDLSC spheroids

Next, to assess the impact of flow on the osteodifferentiation potential of PDLSC spheroids, we cultured the spheroids in osteoinductive culture media under static and flow conditions. After 14 days, alizarin red staining revealed markedly higher staining intensity under flow conditions compared to static conditions (Fig. 5A and B). Further, spheroids under high-flow conditions exhibited significantly stronger staining than low-flow conditions. To validate these findings, we used fluorescent labeling with a calcium binding agent BoneTag to visualize calcium deposits within the spheroids. This enabled the visualization and qualitative comparison of the calcium deposits under different *z*-planes within the spheroids (Fig. 5C). In superficial planes ($z$ = 20 µm from the outer surface), we observed a nearly uniform distribution of calcium staining across the periphery and central regions of the spheroids among all the conditions. However, the calcium deposits appeared to be more in high-flow conditions compared to low-flow and static conditions. In contrast, in the deeper planes ($z$ = 50 µm from the outer surface), the staining patterns were distinct among the conditions. Spheroids cultured under static conditions displayed calcium staining primarily restricted to peripheral zone. Conversely, spheroids cultured under flow conditions exhibited uniform calcium staining across the per-

 

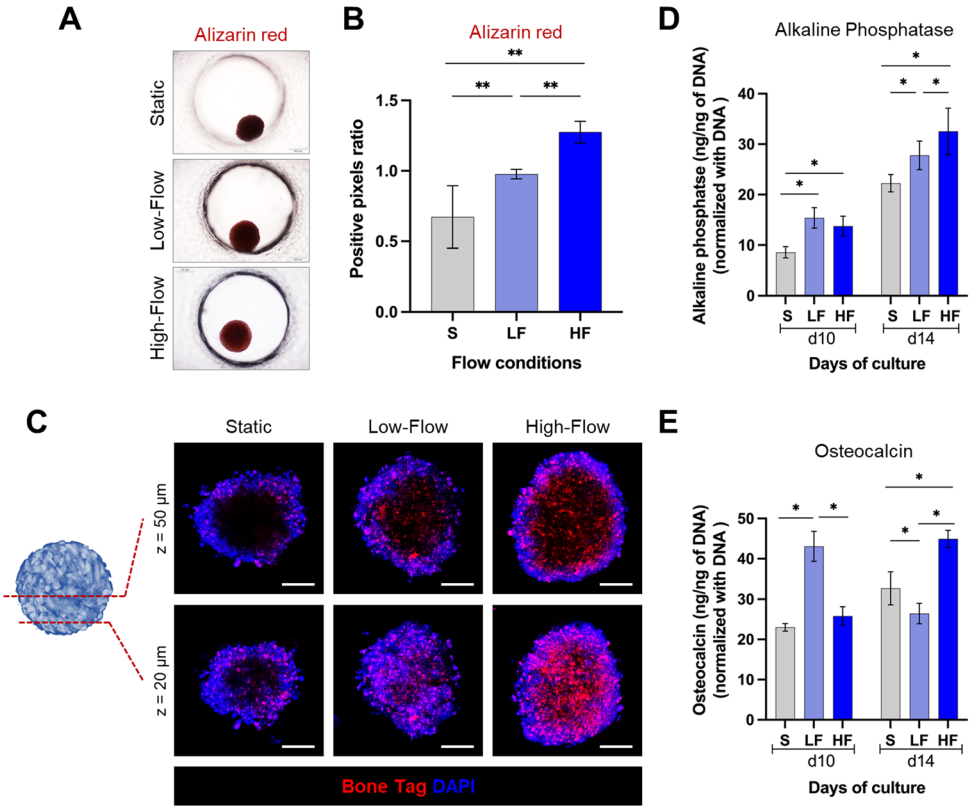


**Fig. 5** Osteodifferentiation potential of PDLSC spheroids under flow conditions. (A) Representative brightfield images and (B) quantification of mean positive pixels ratio of alizarin red-stained PDLSC spheroids after 14 days of culture under osteodifferentiation medium and different flow conditions on-chip (Scale bar 200 µm). (C) Representative confocal *z*-sections of PDLSC spheroids (after 14 days of culture under osteodifferentiation medium) and stained with calcium-binding agent BoneTag (red) and DAPI (blue). The panels represent superficial and deeper *z*-sections of the spheroids to visualize the calcium deposits within peripheral and deeper zones (scale bar: 100 µm). Graphs showing the quantification of (D) intracellular alkaline phosphatase and (E) osteocalcin levels (normalized with respective DNA contents) after 10 and 14 days of culture under osteodifferentiation media and different flow conditions on-chip. (Data presented as mean ± SD, $*p < 0.05$, $** p < 0.01$, $n \geq 4$) (S: static, LF: low-flow, HF: high-flow).

iphery and central zones. Additionally, the staining pattern was more pronounced under high-flow conditions compared to low-flow conditions. These findings were further corroborated by the significantly higher amounts of intracellular alkaline phosphatase under flow conditions compared to static conditions on both day 10 and day 14 (Fig. 5D). Further, the alkaline phosphatase levels on day 14, were significantly higher under high-flow conditions compared to low-flow conditions. However, the low-flow conditions displayed significantly high levels of intracellular osteocalcin on day 10 compared to static and high-flow conditions, while on day 14, low-flow conditions resulted in the lowest levels, followed by static and high-flow conditions (Fig. 5E). Overall, these findings suggest the enhanced osteodifferentiation under flow conditions.

## Discussion

Mimicking the microenvironment and regeneration of the PDL and surrounding alveolar bone requires the recapitulation of cell–cell interactions in a 3D microenvironment and under the influence of mechanical stress induced by interstitial fluid flow. In recent years, the integration of microfluidic technology as a versatile tool to simulate the microenvironment of dental and periodontal tissues in both healthy and diseased states, combining fluid flow, cells, biomaterials, and microbes, has gained significant traction.[47] In this study, we leveraged on a microfluidic perfusion array to culture PDLSC spheroids and investigate the impact of interstitial fluid flow on morphogenesis, cellular viability, and osteogenic differentiation of PDLSC spheroids. Computational analysis demonstrated the translation of fluid flow rates of 1.2 µl $min^{-1}$ (low-flow) and 7.2 µl $min^{-1}$ (high-flow) to maximum fluid shear stress of 59 µPa and 360 µPa for low and high-flow conditions, respectively. Despite the extremely low fluid shear rates in both low and high-flow conditions, they resulted in the formation of larger spheroids with enhanced cellular viability and osteodifferentiation potential compared to static conditions. Further, high-flow conditions exhibited a trend towards higher viability, osteodifferentiation and maturation of PDLSC spheroids when compared to low-flow conditions.

Understanding the role of interstitial fluid flow on PDL and alveolar bone tissue homeostasis and regeneration is of significant interest in the field of periodontal biology and tissue engineering.[10] Interstitial fluid flow plays a crucial role in maintaining tissue homeostasis by facilitating nutrient and oxygen delivery, waste removal, and the transport of signaling molecules. In the context of the periodontium, which includes the PDL and alveolar bone, interstitial fluid flow is influenced by physiological forces such as masticatory loading, tooth movement, and mechanical loading on the tooth-supporting structures.[10] PDL and bone cells are sensitive to flow-induced shear stress influencing cytoskeletal and ECM remodeling, immunoregulation and differentiation through mechanotransduction effects.[21–23] Intermittent flow of interstitial fluid following mechanical loading and pulsatile vascular pressure play a crucial role in flow-induced mechanotransduction and its downstream effects on homeostasis and remodeling of PDL and bone.[57] In the current study, to mimic the intermittent activation of the spheroids within the microfluidic perfusion chip, a defined low pulse rate (0.88 per minute) was used to deliver pulsatile flow conditions. Intermittent flow with rest periods, as opposed to continuous flow, was found to enhance matrix deposition and promote stronger osteodifferentiation of mesenchymal progenitor cells cultured over a patterned polymer scaffold encapsulated within a microfluidic chip.[58] Further, intermittent flow profiles enable a resetting of signaling pathways, preventing them from becoming saturated and facilitating their reactivation upon resumption of flow.[58,59]

Towards emulating the 3D microenvironment, cells cultured as spheroids, over microcarriers or within porous scaffolds are increasingly being used in research. However, 3D cultures are commonly limited by poor nutrient perfusion and a hypoxic core.[38,39] To address these limitations, studies have employed various bioreactor,[40,41] flow perfusion[42,43] and microfluidic[44,58,60] systems to enable dynamic culture conditions, improve nutrient perfusion, enhance osteogenesis, and better mimic the native microenvironment. While perfusion studies on 3D cultures have focussed on osteoblasts and bone marrow-derived MSCs, there is paucity of knowledge using PDL-derived cell types including PDLSCs. In the current work, the PDLSC spheroids cultured under static and flow conditions progressively reduced in size over the first 3 days. This could be attributed to cellular compaction within the spheroids.[61] Despite frequent changes of culture media, the PDLSC spheroids under static conditions progressively decreased in size, demonstrated higher cell death in the deeper *z*-planes and higher caspase 3/7 activity. In contrast, the PDLSC spheroids cultured under flow conditions (both low and high) were observed to be larger with higher DNA content, decreased cell death, and lower caspase 3/7 activity compared to static conditions. In static culture conditions, constraints on diffusion limits and mass transport of nutrients to the inner regions of the spheroids result in a necrotic core depending on the spheroid size.[32,38] In contrast, active media perfusion in flow conditions potentially aided enhanced influx of nutrients including oxygen, and efflux of metabolic wastes within the spheroids leading to increased cell viability and larger spheroid size.[38,62,63]

Studies have demonstrated that the fluid shear stress induced by dynamic culture conditions enhance the osteogenic differentiation of various MSCs and osteoblastic cell lines cultured on monolayer[27–31,64,65] and on/within 3D substrates.[40,58,60,66,67] Fluid shear stress has been proposed to promote the osteogenic differentiation of MSCs by initiating a cascade of events, that include stimulation and mechanosensing through ion channels and integrins, transduction of mechanical signals into intracellular biochemical signals through matrix metalloproteinases, and activation of transcription factors to regulate osteogenic gene expression.[68] However, the mechanoresponsive behaviour of MSCs in response to extremely low fluid shear stress representative of physiological levels within the soft tissues is still elusive. Previous studies within microfluidic[60,65] and rotary shakers,[64] have demonstrated that continuous low-magnitude shear stresses (<63 μPa) on monolayer cultured osteoblastic cells promote proliferation and osteogenic differentiation.[60,64,65] Utilizing a hydraulic resistance-based microfluidic chip, a previous study revealed that MSCs cultured as monolayers displayed notable osteogenic differentiation in response to physiologically relevant low fluid shear stress spanning from 1000 to 10 μPa, with behaviour similar to static cultures at levels in the range of 1 μPa.[18] Fluid shear stress within the range of 1.5–52.6 μPa applied continuously for 24 hours on pre-osteoblast cells (MC3T3-E1) monolayers within a microfluidic chip, increased cell proliferation and differentiation,[65] while stress levels higher than 412 μPa inhibited osteoblastic differentiation.[65,69] In contrast to continuous flow, intermittent flow with rest periods was found to promote stronger osteodifferentiation of mesenchymal progenitor cells cultured over a patterned polymer scaffold encapsulated within a microfluidic chip that generated shear stress levels of 0.8–1.4 Pa.[58] Overall, in the literature, a wide range of magnitude of fluid shear stresses have been documented to affect proliferation and differentiation of osteoblastic cell lineages. However, it is difficult to directly compare the results of the current study owing to a number of factors that include different cell types, shear stress magnitude, exposure times, flow type (continuous or pulsatile), culture media and cellular microenvironment (monolayer or 3D).

While both flow conditions in the current study promoted osteogenic differentiation compared to static cultures, particularly within the physiological range of low fluid shear stress, high-flow conditions (360 μPa) exhibited a noticeable trend towards higher viability, osteodifferentiation and maturation of PDLSC spheroids compared to low-flow conditions (59 μPa). Importantly, the fluorescent-based imaging using BoneTag revealed homogenous areas of mineralization in both peripheral and core regions under flow conditions, in contrast to only a peripheral zone of mineralization observed under static conditions. These differences could be attributed to the enhanced diffusion of the nutrients and osteogenic factors into the spheroid core facilitated by flow conditions. However,

 

the flow conditions exhibited heterogeneous temporal effects on intracellular osteocalcin expression levels. While osteocalcin levels gradually increased from day 10 to day 14 under high-flow conditions, spheroids under low-flow exhibited significantly elevated osteocalcin levels, followed by sharp decline at a later time point. This phenomenon may be attributed to differences in nutrient diffusion between the low-flow and high-flow conditions, and the potential compromise of nutrient diffusion into spheroids after initial mineralization. While most studies report enhanced osteodifferentiation under flow conditions,[70] some have yielded contradictory findings, indicating reduced or no change in osteocalcin expression levels despite an increase in alkaline phosphatase expression.[71,72]

One of limitation of this study is the inclusion of osteogenic factors in the culture medium. When spheroids were cultured without osteogenic factors under static and flow conditions, no discernible differences in alkaline phosphatase levels were observed (ESI Fig. 2†), and osteocalcin levels remained below the detection limits (data not shown). The lack of discernible osteodifferentiation under culture media without osteogenic factors in this study could be due to extremely low fluid shear stress levels used in this study. Secondly, owing to the chip design, relatively high flow rates were used to generate the low fluid shear rates experienced by the spheroids in the niche area of the microwells. Although continuous perfusion enhances nutrient transport and waste removal, sustained perfusion under unidirectional high flow rates might deplete autocrine and paracrine factors, potentially leading to reduced osteoblastic differentiation.[69,73] Prior studies investigating the influence of flow on osteodifferentiation in both monolayer and 3D cultures, without the inclusion of osteogenic factors, have typically employed perfusion systems with high fluid shear stress and circuit designs with recirculation. However, previous studies involving MSCs, whether cultured as monolayers and seeded on electrospun scaffolds utilizing rocker platforms[74,75] or cultured within 3D polymer scaffolds within microfluidic devices,[58] have demonstrated that while fluid shear stress may enhance osteogenic differentiation, but alone is not sufficient under *in vitro* conditions. Future studies could employ modified microfluidic designs that allow for direct perfusion of media into PDLSC spheroids or PDLSCs embedded within hydrogels or scaffolds. Additionally, circuit designs with recirculation of the culture media or the utilization of gravity-driven pumpless microfluidic design on rocker platforms may help mitigate the limitations and provide valuable insights into the effects of low interstitial fluid flow-induced shear stress on PDLSCs.

## Conclusions

In this study, we employed a microfluidic spheroid culture platform to investigate the effects of modulation of fluid flow on PDLSC spheroids. The microfluidic platform provided a physiologically relevant microenvironment with controlled flow conditions. Fluid flow influenced the morphology of the spheroids, promoting larger spheroids with enhanced cellular viability. Moreover, the spheroids cultured under flow conditions (both low and high) exhibited increased osteodifferentiation potential compared to static conditions, with low-flow conditions showing early induction of osteodifferentiation. Overall, this study highlights the significance of fluid flow modulation on PDLSC spheroids and represents a significant step towards the establishment of more complex and physiologically relevant *in vitro* periodontal models. Future investigations focusing on the interplay between flow-mediated interactions of PDLSC spheroids with the microbiome and biomaterials hold great potential for advancing our understanding of periodontal pathophysiology and facilitating the screening and development of innovative periodontal therapeutics, tissue engineering approaches, and regenerative applications.

## Author contributions

Apurva Mishra: conceptualization, methodology, formal analysis, data curation, visualization. Investigation, writing – original draft, Ren Kai: methodology, software, formal analysis, writing – review and editing. Srividya Atkuru: methodology, investigation, writing – review and editing. Yichen dai: methodology, investigation, writing – review and editing. Filippo Piccinini: methodology, investigation, software, visualization, writing – review and editing. Philip Preshaw: supervision, funding acquisition, writing – review and editing. Gopu Sriram: conceptualization, writing – review and editing, supervision, project administration, funding acquisition, resources, visualization.

## Conflicts of interest

There are no conflicts of interest to declare.

## Acknowledgements

This work was partially supported by grants from Academic Research funds (A-0002084-00-00) from National University of Singapore and Singapore Ministry of Education, and Fellowship for Young Professor (FLY) Programme by NUS Centre for Additive Manufacturing (Project ID: AMNUS-2021-008). Apurva Mishra is supported by NUS Research Scholarship. The authors would like to express their gratitude to Ms. Lee Shu Ying, Confocal Microscopy Unit, National University of Singapore and Dr Ma Xiaoxiao, A*STAR Microscopy Platform for their invaluable assistance and support with confocal microscopy.

## References

1 N. J. Kassebaum, E. Bernabe, M. Dahiya, B. Bhandari, C. J. Murray and W. Marcenes, Global burden of severe periodontitis in 1990-2010: a systematic review and meta-regression, *J. Dent. Res.*, 2014, **93**(11), 1045–1053.

2 P. E. Petersen and H. Ogawa, The global burden of periodontal disease: towards integration with chronic disease prevention and control, *Periodontol 2000*, 2012, **60**(1), 15–39.
3 D. Trindade, R. Carvalho, V. Machado, L. Chambrone, J. J. Mendes and J. Botelho, Prevalence of periodontitis in dentate people between 2011 and 2020: A systematic review and meta-analysis of epidemiological studies, *J. Clin. Periodontol.*, 2023, **50**(5), 604–626.
4 J. Botelho, V. Machado, Y. Leira, L. Proença, L. Chambrone and J. J. Mendes, Economic burden of periodontitis in the United States and Europe: An updated estimation, *J. Periodontol.*, 2022, **93**(3), 373–379.
5 B. K. Connizzo, L. Sun, N. Lacin, A. Gendelman, I. Solomonov, I. Sagi, *et al.*, Nonuniformity in Periodontal Ligament: Mechanics and Matrix Composition, *J. Dent. Res.*, 2021, **100**(2), 179–186.
6 C. A. McCulloch, P. Lekic and M. D. McKee, Role of physical forces in regulating the form and function of the periodontal ligament, *Periodontol 2000*, 2000, **24**, 56–72.
7 S. S. Jin, D. Q. He, Y. Wang, T. Zhang, H. J. Yu, Z. X. Li, *et al.*, Mechanical force modulates periodontal ligament stem cell characteristics during bone remodelling via TRPV4, *Cell Proliferation*, 2020, **53**(10), e12912.
8 F. Liu, F. Wen, D. He, D. Liu, R. Yang, X. Wang, *et al.*, Force-Induced H(2)S by PDLSCs Modifies Osteoclastic Activity during Tooth Movement, *J. Dent. Res.*, 2017, **96**(6), 694–702.
9 J. M. Ferrier and E. M. Dillon, The water binding capacity of the periodontal ligament and its role in mechanical function, *J. Periodontal Res.*, 1983, **18**(5), 469–473.
10 M. Ashrafi, F. Ghalichi, B. Mirzakouchaki and I. Zoljanahi Oskui, Numerical simulation of hydro-mechanical coupling of periodontal ligament, *Proc. Inst. Mech. Eng., Part H*, 2020, **234**(2), 171–178.
11 E. H. Burger and J. Klein-Nulend, Mechanotransduction in bone–role of the lacuno-canalicular network, *FASEB J.*, 1999, **13**(Suppl), S101–S112.
12 J. Rubin, C. Rubin and C. R. Jacobs, Molecular pathways mediating mechanical signaling in bone, *Gene*, 2006, **367**, 1–16.
13 Y. Li, M. Li, L. Tan, S. Huang, L. Zhao, T. Tang, *et al.*, Analysis of time-course gene expression profiles of a periodontal ligament tissue model under compression, *Arch. Oral Biol.*, 2013, **58**(5), 511–522.
14 Y. Wang, Y. Li, X. Fan, Y. Zhang, J. Wu and Z. Zhao, Early proliferation alteration and differential gene expression in human periodontal ligament cells subjected to cyclic tensile stress, *Arch. Oral Biol.*, 2011, **56**(2), 177–186.
15 A. Saminathan, G. Sriram, J. Vinoth, T. Cao and M. Meikle, Engineering the periodontal ligament in hyaluronangelatintype I collagen constructs: upregulation of apoptosis and alterations in gene expression by cyclic compressive strain, *Tissue Eng., Part A*, 2014, **21**(3–4), 518–529.
16 M. T. van der Pauw, J. Klein-Nulend, T. van den Bos, E. H. Burger, V. Everts and W. Beertsen, Response of periodontal ligament fibroblasts and gingival fibroblasts to pulsating fluid flow: nitric oxide and prostaglandin E2 release and expression of tissue non-specific alkaline phosphatase activity, *J. Periodontal Res.*, 2000, **35**(6), 335–343.
17 J. M. Rutkowski and M. A. Swartz, A driving force for change: interstitial flow as a morphoregulator, *Trends Cell Biol.*, 2007, **17**(1), 44–50.
18 X. Gao, X. Zhang, H. Xu, B. Zhou, W. Wen and J. Qin, Regulation of cell migration and osteogenic differentiation in mesenchymal stem cells under extremely low fluidic shear stress, *Biomicrofluidics*, 2014, **8**(5), 052008.
19 C. M. Franca, G. S. Balbinot, D. Cunha, V. P. A. Saboia, J. Ferracane and L. E. Bertassoni, In vitro models of biocompatibility testing for restorative dental materials: From 2D cultures to organs on-a-chip, *Acta Biomater.*, 2022, **150**, 58–66.
20 V. Rosa, G. Sriram, N. McDonald and B. N. Cavalcanti, A critical analysis of research methods and biological experimental models to study pulp regeneration, *Int. Endod. J.*, 2022, **55**(Suppl 2), 446–455.
21 L. Zheng, Y. Huang, W. Song, X. Gong, M. Liu, X. Jia, *et al.*, Fluid shear stress regulates metalloproteinase-1 and 2 in human periodontal ligament cells: involvement of extracellular signal-regulated kinase (ERK) and P38 signaling pathways, *J. Biomech.*, 2012, **45**(14), 2368–2375.
22 M. Tang, Z. Peng, Z. Mai, L. Chen, Q. Mao, Z. Chen, *et al.*, Fluid shear stress stimulates osteogenic differentiation of human periodontal ligament cells via the extracellular signal-regulated kinase 1/2 and p38 mitogen-activated protein kinase signaling pathways, *J. Periodontol.*, 2014, **85**(12), 1806–1813.
23 R. Suwittayarak, N. Klincumhom, U. Ngaokrajang, W. Namangkalakul, J. N. Ferreira, P. Pavasant, *et al.*, Shear Stress Enhances the Paracrine-Mediated Immunoregulatory Function of Human Periodontal Ligament Stem Cells via the ERK Signalling Pathway, *Int. J. Mol. Sci.*, 2022, **23**(13), 7119.
24 A. Maeda, K. Soejima, K. Bandow, K. Kuroe, K. Kakimoto, S. Miyawaki, *et al.*, Force-induced IL-8 from periodontal ligament cells requires IL-1beta, *J. Dent. Res.*, 2007, **86**(7), 629–634.
25 N. Klincumhom, C. Lorthongpanich, K. Thumanu, P. Septham, W. Phomyu, S. Issaragrisil, *et al.*, Intermittent compressive force regulates human periodontal ligament cell behavior via yes-associated protein, *Heliyon*, 2022, **8**(10), e10845.
26 L. Qi and Y. Zhang, The microRNA 132 regulates fluid shear stress-induced differentiation in periodontal ligament cells through mTOR signaling pathway, *Cell. Physiol. Biochem.*, 2014, **33**(2), 433–445.
27 J. Song, L. Liu, L. Lv, S. Hu, A. Tariq, W. Wang, *et al.*, Fluid shear stress induces Runx-2 expression via upregulation of PIEZO1 in MC3T3-E1 cells, *Cell Biol. Int.*, 2020, **44**(7), 1491–1502.
28 L. Yu, X. Ma, J. Sun, J. Tong, L. Shi, L. Sun, *et al.*, Fluid shear stress induces osteoblast differentiation and arrests the cell cycle at the G0 phase via the ERK1/2 pathway, *Mol. Med. Rep.*, 2017, **16**(6), 8699–8708.

 

29 K. M. Kim, Y. J. Choi, J.-H. Hwang, A. R. Kim, H. J. Cho, E. S. Hwang, *et al.*, Shear stress induced by an interstitial level of slow flow increases the osteogenic differentiation of mesenchymal stem cells through TAZ activation, *PLoS One*, 2014, **9**(3), e92427.

30 G. Yourek, S. M. McCormick, J. J. Mao and G. C. Reilly, Shear stress induces osteogenic differentiation of human mesenchymal stem cells, *Regener. Med.*, 2010, **5**(5), 713–724.

31 P. Becquart, M. Cruel, T. Hoc, L. Sudre, K. Pernelle, R. Bizios, *et al.*, Human mesenchymal stem cell responses to hydrostatic pressure and shear stress, *Eur. Cells Mater.*, 2016, **31**, 160–173.

32 B. L. Yen, C. C. Hsieh, P. J. Hsu, C. C. Chang, L. T. Wang and M. L. Yen, Three-Dimensional Spheroid Culture of Human Mesenchymal Stem Cells: Offering Therapeutic Advantages and In Vitro Glimpses of the In Vivo State, *Stem Cells Transl. Med.*, 2023, **12**(5), 235–244.

33 A. Imamura, H. Kajiya, S. Fujisaki, M. Maeshiba, T. Yanagi, H. Kojima, *et al.*, Three-dimensional spheroids of mesenchymal stem/stromal cells promote osteogenesis by activating stemness and Wnt/beta-catenin, *Biochem. Biophys. Res. Commun.*, 2020, **523**(2), 458–464.

34 Y. Moritani, M. Usui, K. Sano, K. Nakazawa, T. Hanatani, M. Nakatomi, *et al.*, Spheroid culture enhances osteogenic potential of periodontal ligament mesenchymal stem cells, *J. Periodontal Res.*, 2018, **53**(5), 870–882.

35 K. Sano, M. Usui, Y. Moritani, K. Nakazawa, T. Hanatani, H. Kondo, *et al.*, Co-cultured spheroids of human periodontal ligament mesenchymal stem cells and vascular endothelial cells enhance periodontal tissue regeneration, *Regener. Med.*, 2020, **14**, 59–71.

36 M. Yamamoto, N. Kawashima, N. Takashino, Y. Koizumi, K. Takimoto, N. Suzuki, *et al.*, Three-dimensional spheroid culture promotes odonto/osteoblastic differentiation of dental pulp cells, *Arch. Oral Biol.*, 2014, **59**(3), 310–317.

37 B. Inanc, A. E. Elcin and Y. M. Elcin, Osteogenic induction of human periodontal ligament fibroblasts under two- and three-dimensional culture conditions, *Tissue Eng.*, 2006, **12**(2), 257–266.

38 K. Moshksayan, N. Kashaninejad, M. E. Warkiani, J. G. Lock, H. Moghadas, B. Firoozabadi, *et al.*, Spheroids-on-a-chip: Recent advances and design considerations in microfluidic platforms for spheroid formation and culture, *Sens. Actuators, B*, 2018, **263**, 151–176.

39 M. Chatzinikolaidou, Cell spheroids: the new frontiers in in vitro models for cancer drug validation, *Drug Discovery Today*, 2016, **21**(9), 1553–1560.

40 S. Li, Z. Ma, Z. Niu, H. Qian, D. Xuan, R. Hou, *et al.*, NASA-approved rotary bioreactor enhances proliferation and osteogenesis of human periodontal ligament stem cells, *Stem Cells Dev.*, 2009, **18**(9), 1273–1282.

41 F. Zhao, B. van Rietbergen, K. Ito and S. Hofmann, Flow rates in perfusion bioreactors to maximise mineralisation in bone tissue engineering in vitro, *J. Biomech.*, 2018, **79**, 232–237.

42 G. N. Bancroft, V. I. Sikavitsas, J. van den Dolder, T. L. Sheffield, C. G. Ambrose, J. A. Jansen, *et al.*, Fluid flow increases mineralized matrix deposition in 3D perfusion culture of marrow stromal osteoblasts in a dose-dependent manner, *Proc. Natl. Acad. Sci. U. S. A.*, 2002, **99**(20), 12600–12605.

43 H. L. Holtorf, J. A. Jansen and A. G. Mikos, Flow perfusion culture induces the osteoblastic differentiation of marrow stroma cell-scaffold constructs in the absence of dexamethasone, *J. Biomed. Mater. Res., Part A*, 2005, **72**(3), 326–334.

44 A. Mansoorifar, R. Gordon, R. Bergan and L. E. Bertassoni, Bone-on-a-chip: microfluidic technologies and microphysiologic models of bone tissue, *Adv. Funct. Mater.*, 2021, **31**(6), 2006796.

45 H. Makkar, Y. Zhou, K. S. Tan, C. T. Lim and G. Sriram, Modeling Crevicular Fluid Flow and Host-Oral Microbiome Interactions in a Gingival Crevice-on-Chip, *Adv. Healthcare Mater.*, 2023, **12**(6), e2202376.

46 G. Sriram, M. Alberti, Y. Dancik, B. Wu, R. Wu, Z. Feng, *et al.*, Full-thickness human skin-on-chip with enhanced epidermal morphogenesis and barrier function, *Mater. Today*, 2018, **21**(4), 326–340.

47 C. Huang, F. Sanaei, W. P. R. Verdurmen, F. Yang, W. Ji and X. F. Walboomers, The Application of Organs-on-a-Chip in Dental, Oral, and Craniofacial Research, *J. Dent. Res.*, 2023, **102**(4), 364–337.

48 E.-J. Lee, Y. Kim, P. Salipante, A. P. Kotula, S. Lipshutz, D. T. Graves, *et al.*, Mechanical Regulation of Oral Epithelial Barrier Function, *Bioengineering*, 2023, **10**(5), 517.

49 L. Jin, N. Kou, F. An, Z. Gao, T. Tian, J. Hui, *et al.*, Analyzing Human Periodontal Soft Tissue Inflammation and Drug Responses In Vitro Using Epithelium-Capillary Interface On-a-Chip, *Biosensors*, 2022, **12**(5), 345.

50 C. M. Franca, A. Tahayeri, N. S. Rodrigues, S. Ferdosian, R. M. Puppin Rontani, G. Sereda, *et al.*, The tooth on-a-chip: a microphysiologic model system mimicking the biologic interface of the tooth with biomaterials, *Lab Chip*, 2020, **20**(2), 405–413.

51 S. Hu, G. Muniraj, A. Mishra, K. Hong, J. L. Lum, C. H. L. Hong, *et al.*, Characterization of silver diamine fluoride cytotoxicity using microfluidic tooth-on-a-chip and gingival equivalents, *Dent. Mater.*, 2022, **38**(8), 1385–1394.

52 H. Makkar, S. Atkuru, Y. L. Tang, T. Sethi, C. T. Lim, K. S. Tan, *et al.*, Differential immune responses of 3D gingival and periodontal connective tissue equivalents to microbial colonization, *J. Tissue Eng.*, 2022, **13**, 20417314221111650.

53 T. Masiello, A. Dhall, L. P. M. Hemachandra, N. Tokranova, J. A. Melendez and J. Castracane, A Dynamic Culture Method to Produce Ovarian Cancer Spheroids under Physiologically-Relevant Shear Stress, *Cells*, 2018, **7**(12), 277.

54 F. Piccinini, A. Tesei and A. Bevilacqua, Single-image based methods used for non-invasive volume estimation of cancer spheroids: a practical assessing approach based on

entry-level equipment, *Comput. Methods Programs Biomed.*, 2016, **135**, 51–60.

55 B. Eggerschwiler, D. D. Canepa, H. C. Pape, E. A. Casanova and P. Cinelli, Automated digital image quantification of histological staining for the analysis of the trilineage differentiation potential of mesenchymal stem cells, *Stem Cell Res. Ther.*, 2019, **10**(1), 69.

56 M. J. Moester, M. A. Schoeman, I. B. Oudshoorn, M. M. van Beusekom, I. M. Mol, E. L. Kaijzel, *et al.*, Validation of a simple and fast method to quantify in vitro mineralization with fluorescent probes used in molecular imaging of bone, *Biochem. Biophys. Res. Commun.*, 2014, **443**(1), 80–85.

57 S. P. Fritton and S. Weinbaum, Fluid and Solute Transport in Bone: Flow-Induced Mechanotransduction, *Annu. Rev. Fluid Mech.*, 2009, **41**, 347–374.

58 H. Bahmaee, R. Owen, L. Boyle, C. M. Perrault, A. A. Garcia-Granada, G. C. Reilly, *et al.*, Design and Evaluation of an Osteogenesis-on-a-Chip Microfluidic Device Incorporating 3D Cell Culture, *Front. Bioeng. Biotechnol.*, 2020, **8**, 557111.

59 X. Gong, Y. Fan, Y. Zhang, C. Luo, X. Duan, L. Yang, *et al.*, Inserted rest period resensitizes MC3T3-E1 cells to fluid shear stress in a time-dependent manner via F-actin-regulated mechanosensitive channel(s), *Biosci., Biotechnol., Biochem.*, 2014, **78**(4), 565–573.

60 E. Babaliari, G. Petekidis and M. Chatzinikolaidou, A Precisely Flow-Controlled Microfluidic System for Enhanced Pre-Osteoblastic Cell Response for Bone Tissue Engineering, *Bioengineering*, 2018, **5**(3), 66.

61 T. J. Bartosh, J. H. Ylostalo, A. Mohammadipoor, N. Bazhanov, K. Coble, K. Claypool, *et al.*, Aggregation of human mesenchymal stromal cells (MSCs) into 3D spheroids enhances their antiinflammatory properties, *Proc. Natl. Acad. Sci. U. S. A.*, 2010, **107**(31), 13724–13729.

62 Y. S. Kim, A. Asif, A. R. Chethikkattuveli Salih, J. W. Lee, K. N. Hyun and K. H. Choi, Gravity-Based Flow Efficient Perfusion Culture System for Spheroids Mimicking Liver Inflammation, *Biomedicines*, 2021, **9**(10), 1369.

63 G. Hu and D. Li, Three-dimensional modeling of transport of nutrients for multicellular tumor spheroid culture in a microchannel, *Biomed. Microdevices*, 2007, **9**(3), 315–323.

64 U. M. Liegibel, U. Sommer, B. Bundschuh, B. Schweizer, U. Hilscher, A. Lieder, *et al.*, Fluid shear of low magnitude increases growth and expression of TGFbeta1 and adhesion molecules in human bone cells in vitro, *Exp. Clin. Endocrinol. Diabetes*, 2004, **112**(7), 356–363.

65 W. Yu, H. Qu, G. Hu, Q. Zhang, K. Song, H. Guan, *et al.*, A microfluidic-based multi-shear device for investigating the effects of low fluid-induced stresses on osteoblasts, *PLoS One*, 2014, **9**(2), e89966.

66 M. Hao, M. Xiong, Y. Liu, W.-s. Tan and H. Cai, Magnetic-driven dynamic culture promotes osteogenesis of mesenchymal stem cell, *Bioresour. Bioprocess.*, 2021, **8**(1), 15.

67 S. W. Huang, S. C. Tzeng, J. K. Chen, J. S. Sun and F. H. Lin, A Dynamic Hanging-Drop System for Mesenchymal Stem Cell Culture, *Int. J. Mol. Sci.*, 2020, **21**(12), 4298.

68 L. Liu, W. Yuan and J. Wang, Mechanisms for osteogenic differentiation of human mesenchymal stem cells induced by fluid shear stress, *Biomech. Model Mechanobiol.*, 2010, **9**(6), 659–670.

69 S. D. Carter, L. Barbe, M. Tenje and G. Mestres, Exploring microfluidics as a tool to evaluate the biological properties of a titanium alloy under dynamic conditions, *Biomater. Sci.*, 2020, **8**(22), 6309–6321.

70 C. Wittkowske, G. C. Reilly, D. Lacroix and C. M. Perrault, In Vitro Bone Cell Models: Impact of Fluid Shear Stress on Bone Formation, *Front. Bioeng. Biotechnol.*, 2016, **4**, 87.

71 M. D. Aisha, M. N. Nor-Ashikin, A. B. Sharaniza, H. Nawawi and G. R. Froemming, Orbital fluid shear stress promotes osteoblast metabolism, proliferation and alkaline phosphates activity in vitro, *Exp. Cell Res.*, 2015, **337**(1), 87–93.

72 A. D. Bakker, B. Zandieh-Doulabi and J. Klein-Nulend, Strontium ranelate affects signaling from mechanically-stimulated osteocytes towards osteoclasts and osteoblasts, *Bone*, 2013, **53**(1), 112–119.

73 D. Ellison, A. Munden and A. Levchenko, Computational model and microfluidic platform for the investigation of paracrine and autocrine signaling in mouse embryonic stem cells, *Mol. BioSyst.*, 2009, **5**(9), 1004–1012.

74 R. M. Delaine-Smith, S. MacNeil and G. C. Reilly, Matrix production and collagen structure are enhanced in two types of osteogenic progenitor cells by a simple fluid shear stress stimulus, *Eur. Cells Mater.*, 2012, **24**, 162–174.

75 S. Puwanun, R. M. Delaine-Smith, H. E. Colley, J. M. Yates, S. MacNeil and G. C. Reilly, A simple rocker-induced mechanical stimulus upregulates mineralization by human osteoprogenitor cells in fibrous scaffolds, *J. Tissue Eng. Regener. Med.*, 2018, **12**(2), 370–381.

76 G. Muniraj, R. H. S. Tan, Y. Dai, R. Wu, M. Alberti and G. Sriram, Microphysiological Modeling of Gingival Tissues and Host-Material Interactions Using Gingiva-on-Chip, *Adv. Healthc. Mater.*, 2023, e2301472.

 